Theoretical and Experimental Study of Radiant Heat Transfer in a Solar Fluidized-Bed Receiver

The temperature profile, total emissivity, flux density distribution, and effective mean penetration distance were determined from measurements in high-temperature solar fluidized beds. A theoretical model is proposed to describe the complex heat transfer phenomena in the radiation penetration zone of the fluidized layers. The results correlated well at incipient fluidizing conditions for beds of silicon carbide and chamotte but were found imprecise for beds of zirconia and silica sand.

G. FLAMANT

Laboratoire d'Energétique Solaire
Odeillo, France

SCOPE

Because of the well-known properties of gas-fluidized bed—high absorptance, uniform temperature distribution, high value of heat transfer coefficient, etc., a solar fluidized bed has been designed (Flamant, 1978). This type of gas-solid receiver may be used to heat gas (gas-cycle solar-power plant) or to process chemicals (preparative chemistry, chemical storage of energy) (Badie et al., 1980).

There are two ways for heating a fluidized bed with concentrated solar radiation: on the one hand, using a transparent column in which the bed acts as a porous absorber; on the other hand, providing the reactor with a metallic wall which transfers heat to the bed by conduction. Flamant et al. (1980) have reported results about the first kind of device; the second one is now under investigation. In both cases, an analysis of the radiative heat exchange inside a bed of particles near its free surface and near the walls must be done.

The present investigation is concerned with the calculation and measure of the temperature profiles of both particles and gas (T,θ) and of the radiant flux density distribution in forward and backward directions (I,J) on the top of the fluidized bed. The proposed theoretical model is an extension of the two-flux theory (Kubelka and Munk, 1931; Hamaker, 1947; Chen and Churchill, 1963) for a gas flowing through a layer of particles (Olalde, 1980). The model and experimental data should be applied to study the radiant heat transfer between a high-temperature source (a wall, for instance) and a fluidized bed.

CONCLUSIONS AND SIGNIFICANCE

A simplified model involving conductive, convective and radiative heat transfer phenomena in porous medium is proposed to describe the high-temperature heat exchange in a fluidized bed. The experimental data deal with beds being subjected to solar beams through a transparent column. The measured extinction coefficient, mean penetration distance, and spectral and total emissivity of various fluidized beds up to 1,200 K may be used to predict radiant heat exchange in particulate fluidized layers or in the emulsion phase of aggregative beds.

At incipient fluidization, the mean penetration distance varies from 3 to 13 particle diameters and the extinction coefficient from 4,500 m^{-1} to 600 m^{-1} according to the bed materials. Some uncertainty exists regarding the experimental data because of the high-temperature source: the power of a solar concentrator is sensitive to minor variations of atmospheric conditions.

Theoretical and experimental data correlate rather well at minimum fluidization conditions (U_o/U_{mf} <1.2). Thus, in future, the theoretical approach will be adapted to study the radiative heat transfer between a fluidized bed and a wall: transient conductive and radiative heat exchange between emulsion packets of solids and a heat emitting wall.

The theoretical analysis can be improved by using a system of band equations taking into account: i) the spectral distribution of incident and emitted radiation; ii) the local variations of the porosity.

INTRODUCTION

According to the experiments of Flamant et al. (1980), the concentrated solar flux entered the reactor through a transparent silica tube and was absorbed in the upper part of the bed. The resulting temperature profile is shown in Figure 1; according to these experimental results, three zones exist in the bed. When cold gas is introduced at the bottom of the reactor, the fluid is heated by the moving hot particles in zone 3 ($\theta < T$). Then, in zone 2, no thermal gradient occurs. In the vicinity of the surface submitted to concentrated radiation, the so-called zone 1 on Figure 1, no experimental data are available because of the light penetration through the porous medium.

When radiation impinges on a bed of particles, a part of the radiation is reflected diffusely, another part is absorbed, and the remainder is transmitted. To describe this phenomena, two types of theories were formulated.

The first one (Bodo, 1951; Melamed, 1963) is based on the granular constitution of the bed and the radiative properties of the powder.

The second type (Kubelka and Munk, 1931; Hamaker, 1947; Chen and Churchill, 1963) involves the absorption and the scattering constants per unit layer thickness. The bed is considered as a continuum.

Relations between these two models were developed by Ter

0001-1541-82-5762-0529-$2.00.

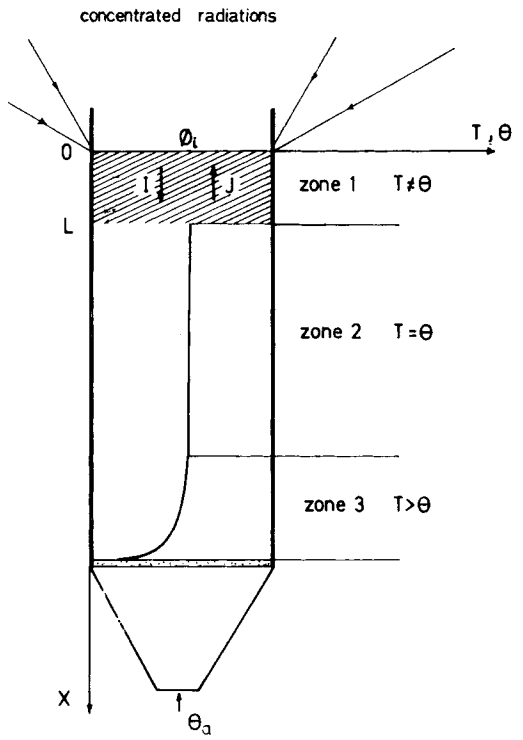

Figure 1. Experimental temperature and distribution in a solar fluidized-bed receiver (Flamant et al., 1980).

Vrugt (1965). Nevertheless, none of them deal with moving powders or gas flowing through the layer. Recently, Olalde et al. (1980) have calculated analytically and numerically the temperature distribution in the solid and the fluid for a gas flowing through a porous material subjected to concentrated solar radiation.

THEORETICAL ANALYSIS

The present theoretical model takes its inspiration from the above-mentioned studies (Chen and Churchill, 1963; Olalde, 1980). The following assumptions are made:

- The fluidized bed is a diffuse grey body.
- The gas is transparent to the radiation.
- The incident radiative flux (ϕ_i) impinging the upper part of the bed is uniform.
- Steady state and one dimensional conditions are supposed.
- The physical properties of fluid and solid are constant.
- The fluidized bed porosity is constant (particulate fluidization).
- The conductive term ($\lambda_F\, d^2\theta/dx^2$) is neglected before the convective one in the energy transfer equation for the gas (Eq. 4).

The radiant transport in the bed is described by integro-differential equations which are solved using the Schuster-Schwarzchild approximation (Siegel and Howel, 1972).

EQUATIONS

The heat balance equations for radiative flux density I, J and for gas and solid temperatures are:

$$\frac{dI}{dx} = -(A + B)I + BJ + A\sigma T^4 \tag{1}$$

$$\frac{dJ}{dx} = (A + B)J - BI - A\sigma T^4 \tag{2}$$

$$A(I + J) + \lambda_b \frac{d^2T}{dx^2} = 2A\sigma T^4 + \frac{(1 - \xi)}{\tau} h(T - \theta) \tag{3}$$

$$\rho_F C_F \xi U \frac{d\theta}{dx} = \frac{(1 - \xi)}{\tau} h(\theta - T) \tag{4}$$

The system may be written:

$$\frac{dI}{dx} = -(A + B)I + BJ + A\sigma T^4 \tag{5}$$

$$\frac{dJ}{dx} = (A + B)J - BI - A\sigma T^4 \tag{6}$$

$$\frac{d^2T}{dx^2} = \frac{A}{\lambda_b}[2\sigma T^4 - (I + J)] + 6\frac{(1 - \xi)}{(f_s d)^2}\mathrm{Nu}\frac{\lambda_F}{\lambda_b}(T - \theta) \tag{7}$$

$$\frac{d\theta}{dx} = \frac{6(1 - \xi)}{f_s d}\frac{\mathrm{Nu}}{\mathrm{RePr}}(\theta - T) \tag{8}$$

A Runge-Kutta computing method is applied to solve the system of five first-order differential equations according to the following boundary conditions.

BOUNDARY CONDITIONS

The following boundary conditions are used:
x = L:

$$I = J = \sigma T_b^4$$

$$T = \theta$$

$$\left.\frac{dJ}{dx}\right|_L = 0$$

$$\left.\frac{d\theta}{dx}\right|_L = 0$$

$x = 0$: the initial values of T, dT/dx, I, J are calculated by the following equations. T_o/ the total heat balance of the reactor may be written:

$$\alpha_b\phi_i = \epsilon_b\sigma(T_o^4 - T_a^4) + \rho_F C_F U_o(\theta_o - \theta_a) + \beta\alpha_b\phi_i \tag{9}$$

We calculated the temperature T_o assuming $T_o = \theta_o$. The last term of the equation $\beta\alpha_b\phi_i$ represents the convective heat loss of the receiver. Experiments with silicon carbide fluidized beds were run at steady-state conditions to achieve the variation of β as a function of T_o: the measured values of ϕ_i, T_o, T_a, θ_o, θ_a, U_o are inserted into Eq. 9 in which α_b and ϵ_b were the parameters.

$dT/dx|_{x=0}$/ on the upper side of the bed, if convective term is neglected, the energy balance is:

$$\alpha_b\phi_i = -\lambda_b^* \left.\frac{dT}{dx}\right|_{x=0} + \epsilon_b\sigma(T_o^4 - T_a^4) \tag{10}$$

with $\lambda_b^* = \lambda_b + \lambda_r$
and

$$\lambda_r = \frac{8\sigma T_o^3}{A + 2B} \text{ (Chen and Churchill, 1963)}$$

I_o,J_o/ the initial value of I is imposed: $I_o = \Phi_i$, then

$$J_o = R_b I_o + \epsilon_b\sigma T_o^4 \tag{11}$$

Equation 11 is solved making the assumption: $\alpha_b = \epsilon_b = 1 - R_b$
θ_o/ with respect to gas temperature θ_o, its value is imposed and corrected according to the boundary conditions for $x = L$.

PARAMETERS

The main parameters of the system are:

- The absorption coefficient A and the scattering coefficient B which are related by the extinction coefficient of directionnal radiation $K = B + A/2$. A and B depend on radiative properties of particles, particles diameter and sphericity, and porosity of the bed. A rough value of B may be estimated from the equation proposed:

i) by Gouffe (1978) for the extinction of light through a cloud of grey particles:

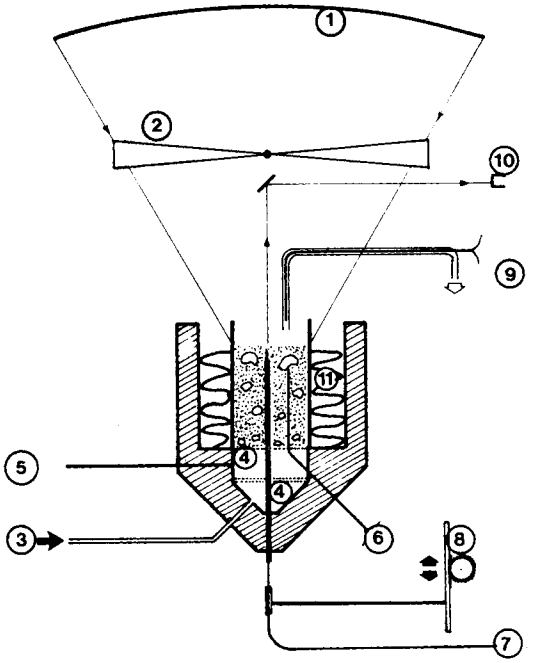

Figure 2. Schematic of experimental apparatus.

1 = Solar Concentrator
2 = Closing Device
3 = Rotameter, Compressed Air
4 = Porous Plate
5 = Pressure Gauge
6 = Thermocouples
7 = Optical Fiber-Photodetector
8 = Optical Fiber Moving Device
9 = Suction Pyrometer
10 = Optical Pyrometer
11 = Insulation

$$B = \frac{k(1-\xi)}{d} \tag{12}$$

and ii) by Siegel and Howel (1972) for specular reflexion in a bed of spheres:

$$B = \frac{3}{2}(1-\xi)\frac{R_p}{d} \tag{13}$$

On the other hand the experimental data of Chen and Churchill (1963) may be used to estimate the ratio B/A.

- The axial effective thermal conductivity of the bed λ_b varies from 170 W/m·K to 4,200 W/m·K according to Lewis et al. (1962) whose data were confirmed by Kunii et al. (1968).
- The heat exchange coefficient between solid and fluidizing gas (air) at low Reynolds number. We use the correlation proposed by Kunii and Levenspiel (1969):

$$\mathrm{Nu} = 0.03\,\mathrm{Re}^{1.3} \tag{14}$$

EXPERIMENTAL APPARATUS AND PROCEDURE

A scheme of the fluidized bed reactor is shown in Figure 2. The solar concentrator is composed of spherical facets. Its power may be modulated from 0.5 to 5.5 kW with a pneumatic device. The flux density profile on the focal plane at maximum power is shown in Figure 3.

The fluidized-bed receiver is composed of a transparent silica tube, 0.065 m diameter × 0.15 m high, inserted in a metallic support. The empty area between these two constituents is filled with mineral insulating wool in order to reduce lateral conductive-convective losses. The gas distributor is a porous Inconel plate. The fluidizing air is introduced at the bottom of the bed at ambient temperature (θ_a = 300 K).

The temperature inside the bed is measured by means of eight bare thermocouples located at the different levels around the axis of the tube. The temperature of the upper part of the bed is measured with an optical pyrometer at $\lambda = 3.4 \times 10^{-6}$ m.

We used a mobile optical fiber (velocity 0.001m/s) connected with a photo-resistant detector put on a diffuse cylinder to measure the extinction of flux density in zone 1. This device allows the measurement of flux I as a function of distance X from irradiated surface. The experimental values

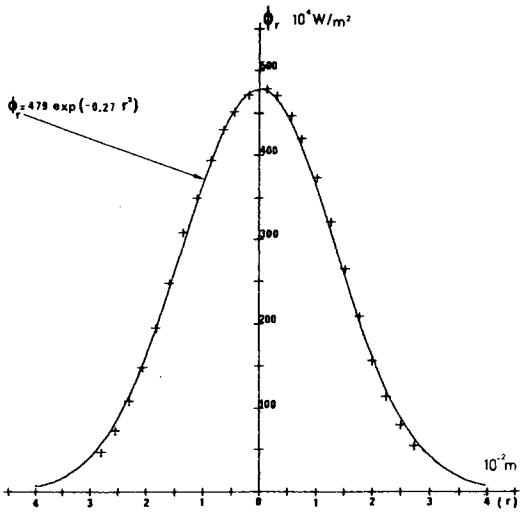

Figure 3. Flux density distribution in the focal plane of the solar concentrator.

of K are obtained through a calibration curve, drawn using a fluxmeter ("Gardon" type).

The fluidized bed ($d = 0.25 \times 10^{-3}$ m, average sieving diameter) is contained in the silica tube and is about 0.01 m high (~350 cm³). We tested four materials: natural silica sand, zirconia, chamotte, and silicon carbide.

The bed spectral emissivity at $\lambda = 3.4 \times 10^{-6}$ m ($\epsilon_{\lambda b}$) is calculated according to the equation (Wien approximation):

$$\frac{1}{T_b} = \frac{1}{T_S} + \frac{\lambda}{C_2} Ln\ \epsilon_{\lambda b} \qquad C_2 = 0.144 \times 10^{-2}\ \mathrm{m{\cdot}K^{-1}} \tag{15}$$

where temperature data are obtained from thermocouples in the plateau zone (T_b) and from the optical pyrometer (T_s).

The steady-state total heat balance (Eq. 9) is solved to calculate the hemispherical total emissivity ϵ_b; α_b, and β are the parameters and the others terms ($\phi_i, T_o \ldots$) are measured.

- Dependance of β on bed temperature T_o:

For various imposed solar flux density, ϕ_i experiments with SiC fluidized beds were run and the values of the variables T_o, θ_o, U_o measured. Then, data are inserted into Eq. 9 using the following values for the parameters α_b and ϵ_b (Figure 5).

$$900\ \mathrm{K} < T_b \leqslant 1{,}250\ \mathrm{K}\ \ \alpha_b = 0.95\ \epsilon_b = 0.85$$
$$1{,}250\ \mathrm{K} < T_b < 1{,}500\ \mathrm{K}\ \ \alpha_b = 0.95\ \epsilon_b = 0.95$$

- Dependance of ϵ_b on bed temperature T_o:

For beds of Zirconia, Silica sand and chamotte particles, ϵ_b vs. T_o is calculated according to Eq. 9 using, as parameters, the values of β shown on Figure 6a, and the values of solar absorptance α_b listed in Table 1.

In Table 1, α_{pb} is the absorptance measured by reflectometry at 300 K on a packed-bed sample; α_b^* is a calculated value according to the correlation (Eq. 16) (Flamant, 1978).

$$\alpha_b^* = \alpha_p / [(1-\xi)(1-\alpha_p) + \alpha_p],\ 0.5 \leqslant \xi \leqslant 0.6 \tag{16}$$

Where the total absorptance at temperature T_b of the bulk material α_p is given by Touloukian and Dewit (1972).

α_b is the final selected value for calculations.

EXPERIMENTAL RESULTS

The dependence of temperature distribution on gas velocity is shown in Figure 4. It should be noticed that a stagnant zone occurs at low gas flow rate ($U/U_{mf} \leqslant 1.3$). The minimum fluidization velocity U_{mf} is calculated at the plateau temperature using the simplified equation (Eq. 17) (Wen and Yu, 1966).

$$U_{mf} = \frac{g(\rho_s - \rho_g)d^2}{1{,}650\,\mu} \qquad \mathrm{Re} < 20 \tag{17}$$

Consequently, experimental tests were conducted using a gas velocity U_o such that $U_o \geqslant 1.5 U_{mf}$. Figure 5 shows the equilibrium temperature of the fluidized bed vs. the mean flux density for the different materials and $1.5 < U_o/U_{mf} < 1.7$.

The measurements do not reveal any temperature increase in the surface vicinity. But, the uncertainty of the experimental data is about ± 20 degrees.

TABLE 1. SELECTED VALUES OF THE ABSORPTANCE OF FLUIDIZED BED

	Zirconia	Silica Sand	Chamotte	Silicon Carbide
α_{pb}	0.25 ± 0.01	0.4 ± 0.02	0.75 ± 0.05	0.91 ± 0.01
α_b^*	0.4 − 0.55	0.45 − 0.60	0.65 − 0.80	0.95 − 1
α_b	0.5 ± 0.05	0.50 ± 0.05	0.75 ± 0.05	0.95 ± 0.05

EMISSIVITY OF THE FLUIDIZED BED

• *Hemispherical Spectral Emissivity* ($\epsilon_{\lambda b}$). The value of $\epsilon_{\lambda b}$ is measured (Eq. 15) for different equilibrium temperatures. No significant variation of the spectral emissivity was observed in the working temperature range, Table 2.

• *Hemispherical total emissivity* (ϵ_b). The experimental results are plotted in Figure 6. A large uncertainty exists because of calculation procedures: for solving Eq. 9, the solar absorptance α_b is estimated and ϕ_i measured with about 10% error.

An increase of the emissivity with the bed temperature is observed by Makhorin et al.; but for spectral data, they noticed that the total emissivity increases with the number of fluidization U/U_{mf}. Our experimental observations can be connected to these results: a change in the mean porosity of the surface (more bubbles breaking into the surface) may create a change of the total emissivity.

• *Mean Penetration Depth.* Measurements were done at low temperatures. Figure 7 shows typical experimental curves. It is noticed that disturbances due to bubbles may be important for $U/U_{mf} > 1.2$. The experimental mean penetration length is given as a function of the number of fluidization U/U_{mf}, Table 3. We used the dimensionless group $L^+ = L/d$. The experimental extinction coefficient deduced from $I(x)$ curves are listed in Table 4.

DISCUSSION

It is impossible to measure with great accuracy the temperature profiles of the particles and of the fluidizing gas near the upper part of the bed. The values measured with thermocouples are intermediate between the solid and the gas temperature. Thus, we cannot confirm the predicted temperature distribution plotted in Figure 8. But, the experimental measures indicate no temperature increase in this zone. Therefore, we can assume that the effective axial thermal conductivity is larger than 100 W/m·K, Figure 8 (Lewis et al., 1962).

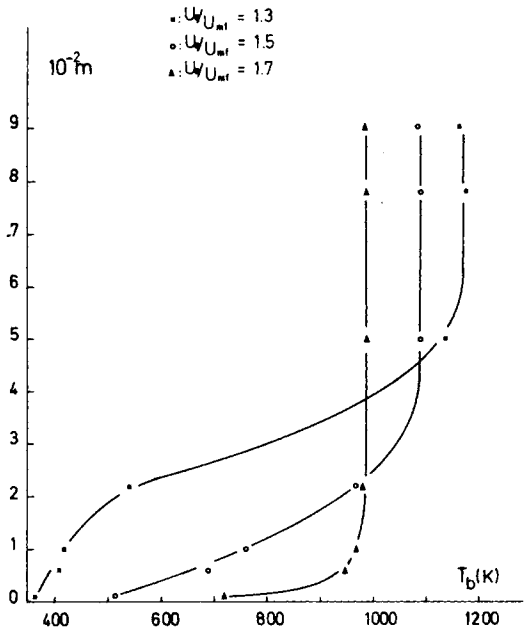

Figure 4. Experimental axial temperature distribution in the fluidized bed vs. number of fluidization: silicon carbide $d = 0.25 \times 10^{-3}$ m; $\phi_i = 20 \times 10^{-4}$W/m².

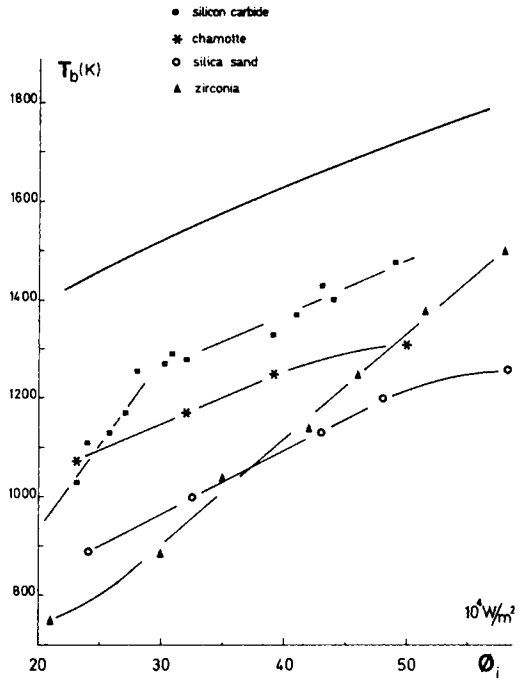

Figure 5. Experimental equilibrium temperature of various fluidized bed vs. mean flux density.

■ Silicon Carbide ▲ Zirconia
* Chamotte ○ Silica Sand
Solid Line = Equilibrium Temperature of Black Body

Theoretical and experimental distributions of I^+ vs. X^+ are plotted in Figures 9 and 10. For $I^+ \geq 0.1$, the computed values of penetration distance are in good agreement with the experimental ones. For $I^+ < 0.1$, the difference is supposed to come from the experimental procedure: tests were carried at ambiant temperature and computation at high temperature ($T > 1{,}100$ K); thus, the radiative emission of the bed ($A\sigma T^4$) is more important for predicted low values of I^+ than for measured ones.

The experimental data correlate very well for highly absorbant media, Figure 9. But, the model is not satisfactory for beds of zirconia or silica sand, Figure 10. This should come from the following theoretical hypothesis.

First, the calculation is based on the constant porosity assumption while in the upper part of the bed ξ decreases from 1 to the mean value ξ_{mf} at incipient fluidization conditions. Consequently, absorption and scattering coefficients increase from 0 to the mean values A and B in this zone.

Secondly, the concentrated solar flux is directional whereas we assume having diffuse conditions inside the bed. This last assumption is right only after several layers of particles.

Finally, low-temperature data are used to compute high-temperature flux density profiles.

When all these phenomena are combined, the experimental flux density is higher than predicted up to point C (Figure 10). Then, the rough calculation hypothesis may be applied.

It should be noticed that experimental data were obtained with

TABLE 2. HEMISPHERICAL SPECTRAL EMISSIVITY OF FLUIDIZED BED $U/U_{mf} = 1.5$

	Zirconia	Silica Sand	Chamotte	Silicon Carbide
Temperature (K) Range	1,300 − 1,500	1,000 − 1,350	1,000 − 1,300	900 − 1,500
$\epsilon_{\lambda b}$	0.3 ± 0.05	0.72 ± 0.03	0.8 ± 0.03	1 ± 0.05

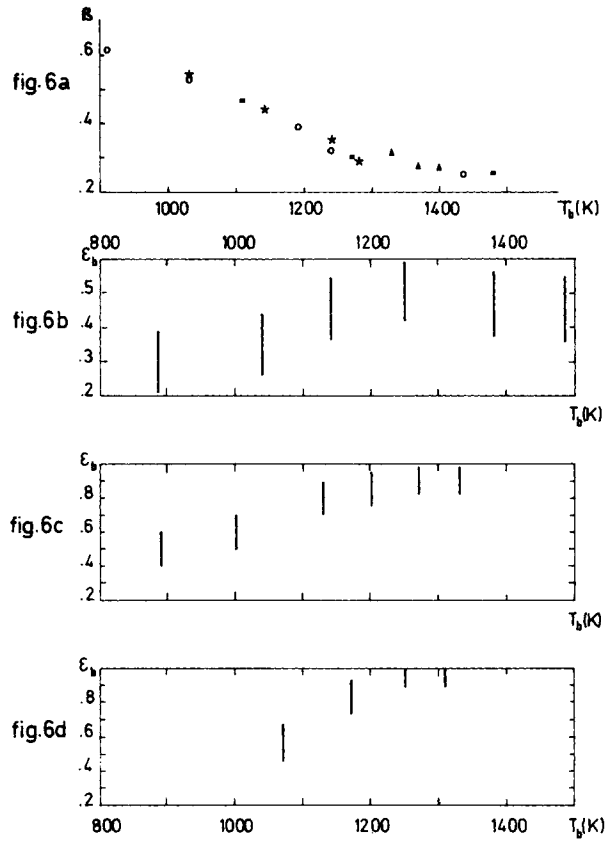

Figure 6. Variation of total emissivity of fluidized bed. For U_o/U_{mf} = 1.5. 6a = experimental value of β (Eq. 9) silicon carbide bed; 6b,c,d, = experimental value of total emissivity vs. bed temperature for zirconia, Silica sand, chamotte respectively $d = 0.25 \times 10^{-3}$ m.

a solar concentrator whose power is sensitive to minor variations of atmospheric conditions.

CONCLUSION

The experimental data for temperature and flux distributions and for mean penetration distance correlate well with computed values, for low fluidization number: $U_o/U_{mf} \leq 1.2$. The results

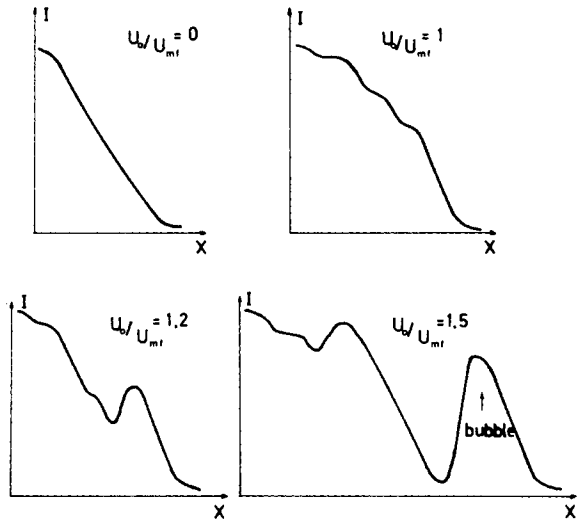

Figure 7. Typical experimental flux density profile for various fluidization numbers, chamotte particles.

TABLE 3. EXPERIMENTAL DIMENSIONLESS MEAN PENETRATION DEPTH OF PACKED AND FLUIDIZED BED $d = 0.25 \times 10^{-3}$m

U/U_{mF}	0	1	1,2	1,5
Silicon Carbide	2.4 ± 0.2	3.2 ± 0.4	3.2 ± 0.6	4.8 ± 0.8
Chamotte	3.2 ± 0.2	3.6 ± 0.4	3.8 ± 0.4	4.8 ± 0.8
Zirconia	11. ± 0.8	13. ± 1.	15. ± 1.2	15. ± 2
Silica Sand	10. ± .8	13. ± 2	16 ± 2	16 ± 2

TABLE 4. EXPERIMENTAL EXTINCTION COEFFICIENT OF PACKED AND FLUIDIZED BED: K(m^{-1}) UNCERTAINTY ± 25%

Fluidization Number	Silicon Carbide	Chamotte	Zirconia	Silica Sand
$U_o/U_{mf} = 0$	5,500	4,500	850	800
$U_o/U_{mf} = 1$	4,000	3,400	600	600

dealing with absorption and scattering coefficient, spectral and total emissivity may be used to predict radiant heat transfer in high-temperature fluidized beds. The differences between measured and computed data may come from the properties of fluidized bed in the surface vicinity and also from the simplifying assumptions adopted for the theorical model.

The theoretical approach should be improved using a system of two bands equations; one in the solar spectral range, the other in the infra-red range, and taking into account the local variations of fluidized-bed porosity.

NOTATION

- I = flux density in positive direction ($W \cdot m^{-2}$)
- J = flux density in negative direction ($W \cdot m^{-2}$)
- A = absorption coefficient per unit length of layer (m^{-1})
- B = scattering coefficient per unit length of layer (m^{-1})
- K = extinction coefficient (m^{-1})
- T = temperature of solid (K)
- d = particle diameter
- h = gas-solid heat transfer coefficient in the fluidized bed ($W \cdot m^{-2} \cdot K^{-1}$)
- C = specific heat ($J \cdot kg^{-1} \cdot K^{-1}$)
- U = average fluid velocity in the axial direction ($m \cdot S^{-1}$)

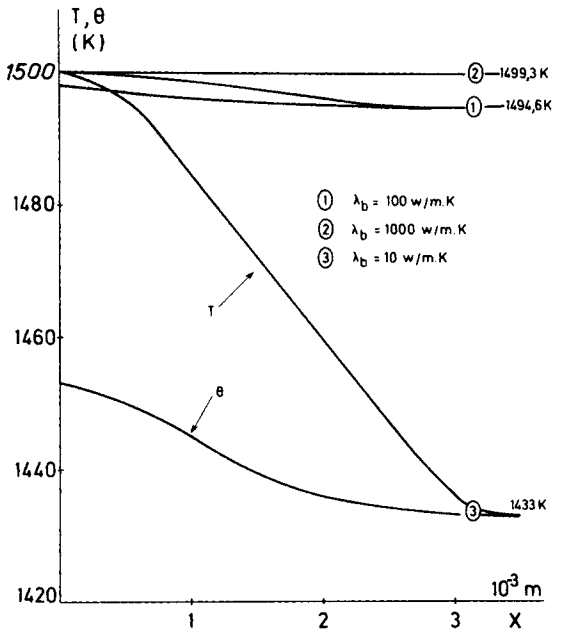

Figure 8. Theoretical particle (T) and gas (θ) temperature profiles vs. thermal conductivity of the bed.
parameters: $\phi_i = 50 \times 10^4 W/m^2$; $\epsilon_b = 0.95$; $B = 2{,}000\ m^{-1}$; $A = 600\ m^{-1}$; $\xi = 0.6$

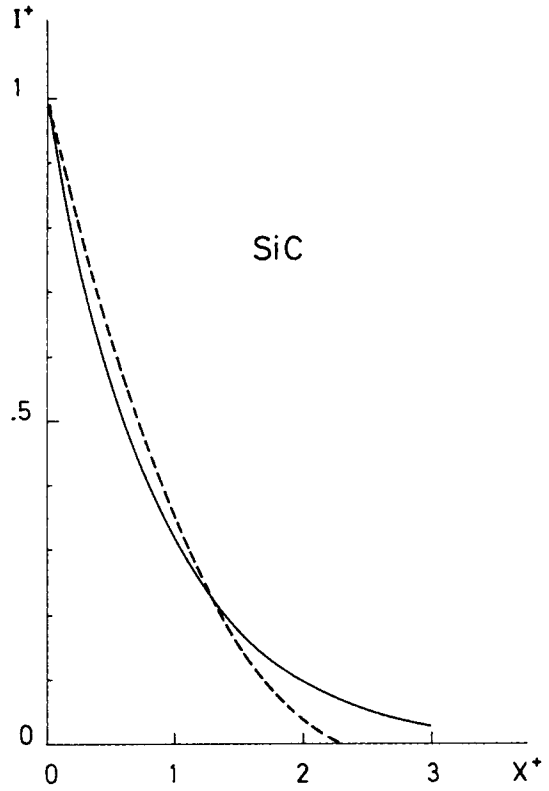

Figure 9. Comparison of computed and measured flux density profiles in a bed of silicon carbide at incipient fluidization conditions: Dotted Curve = Experimental; Solid Line = Calculation; Parameters = $B = 3{,}500\ m^{-1}$, $A = 1{,}000\ m^{-1}$, $\xi = 0.5$, $\epsilon_b = 0.95$.

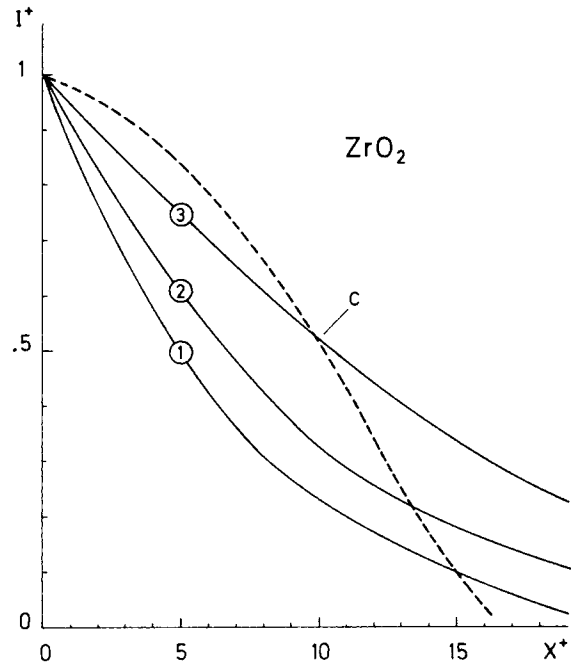

Figure 10. Comparison of computed and measured flux density profiles in a bed of zirconia at incipient fluidization conditions: Dotted Curve = Experimental.

(1)	(2)	(3)
$B = 600\ m^{-1}$	$B = 500\ m^{-1}$	$B = 300\ m^{-1}$
$A = 20\ m^{-1}$	$A = 5\ m^{-1}$	$A = 5\ m^{-1}$
$\xi = 0.5$	$\xi = 0.6$	$\xi = 0.6$
$\epsilon_b = 0.7$	$\epsilon_b = 0.6$	$\epsilon_b = 0.65$

U_o = fluid velocity in the empty column, $U_o = \xi U$
U_{mf} = gas velocity for minimum fluidizing conditions at the equilibrium temperature of the *bed* T_b ($m \cdot S^{-1}$)
L = mean penetration distance (m)
f_s = shape factor = 0.7 For calculation
R = hemispherical reflectivity

Greek Letters

θ = gas temperature (K)
λ_b = axial effective thermal conductivity of the fluidized bed ($W \cdot m^{-1} \cdot K^{-1}$)
λ_r = radiant thermal conductivity of the bed ($W \cdot m^{-1} \cdot K^{-1}$)
$\lambda_b^* = \lambda_b + \lambda_r$
ξ = porosity of the bed
τ = characteristic length of the particles, $\tau = f_s d/6$ (m)
Φ or ϕ = flux density ($W \cdot m^{-2}$)
ρ = density ($kg \cdot m^{-3}$)
ϵ = hemispherical emissivity
α = solar absorptance
μ = viscosity ($N \cdot S \cdot m^{-2}$)
σ = Stefan Boltzman constant, $5{,}675\ 10^{-8}\ W \cdot m^{-2} \cdot K^{-4}$
β = $\dfrac{\text{convective heat losses}}{\text{absorbed solar flux}}$

Subscripts

b = fluidized bed
p = particle
F = fluid (air)
s = Surface
i = incident (on the upper surface of the bed)
a = ambiant
o = irradiated top of the bed
λ = spectral property
mf = incipient fluidization conditions

Dimensionless Groups

$\mathbf{Re} = \dfrac{\rho_F (f_s d) U_o}{\mu}$ Reynolds Number

$\mathrm{Nu} = \dfrac{h(f_s d)}{\lambda_F}$ Nusselt Number

$\mathrm{Pr} = \dfrac{\mu C_F}{\lambda_F}$ Prandlt Number

$I^+ = \dfrac{I - I_1}{I_o - I_1}$, $I_1 = \sigma T^4$

$X^+ = \dfrac{X}{d}$

LITERATURE CITED

Badie, J. M., C. Bonet, M. Faure, G. Flamant, R. Foro, and D. Hernandez, "Decarbonation of Calcite and Phosphate Rock in Solar Chemical Reactors," *Chem. Eng. Sci.*, **35**, p. 413 (1980).

Bodo, Z., "Some Optical Properties of Luminescent Powders," *Acta Phys. Hung.*, **1**, p. 135 (1951).

Chen, J. C. and S. W. Churchill, "Radiant Heat Transfer in Packed Beds," *AIChE J.*, **9**, No. 1, p. 35 (1963).

Flamant, G., "Thermochimie Solaire, Étude de Procédés: Application à la Décarbonatation de la Calcite," Thesis, Université Paul Sabatier (31), Toulouse (1978).

Flamant, G., D. Hernandez, C. Bonet, and J. P. Traverse, "Experimental Aspect of the Thermochemical Conversion of Solar Energy, Decarbonation of $CaCo_3$," *Solar Energy*, **24**, No. 4, p. 385 (1980).

Gouffe, A., "Transmission de la Chaleur par Rayonnement," Col. ANRT SFT ed., Eyrolles (1978).

Hamaker, H. C., "Radiation and Heat Conduction in Light Scattering Material," *Philips. Res. Repts.*, **2**, p. 55, p. 103, p. 112 (1947).

Kubelka, P. and F. Munk, "Ein Beitak zur Optik der Ferbanstriche," *Zeistschrift für Technische Physik.*, No. 11, p. 593 (1931).

Kunii, D., and O. Levenspiel "Fluidization Engineering," Wiley (1969).
Kunii, D., K. Yoshida, and O. Levenspiel, "Axial Movement of Solids in Bubbling Fluidized Solids Beds," *I. Chem. E. Symp. Ser.*, no. 30, p. 79 (1968).
Lewis, W. K., E. R. Gilliland, and H. Girouard, "Heat Transfer and Solids Mixing in Beds of Fluidized Solids," *Chem. Eng. Prog. Symp. Ser.*, no. 38 **58**, p. 87 (1962).
Makhorin, K. E., V. S. Pikashov, and G. P. Kuchin, "Measuring Particle Temperature and Emissivity in a High Temperature Fluidized Bed," *Fluidization*, Proceedings of the 2nd Eng. Fond. Conf., Cambridge University Press, p. 93 (1978).
Melamed, N. T., "Optical Properties of Powders: Part I. Optical Absorption," *J. of Applied Physics*, **34**, No. 3, p. 560 (1963).
Olalde, G., J. L. Peube, and M. Daguenet, "Theoretical Study of Gas Heated in a Porous Material Subjected to a Concentrated Solar Radiation," *Revue de Physique Appliquée*, **15**, p. 423 (1980).
Siegel, R., and J. R. Howel, "Thermal Radiation Heat Transfer," McGraw Hill (1972).
Ter Vrugt, "Optical Properties of Thin Powder Layers," Philips Res. Repts., **20**, p. 23 (1965).
Touloukian, Y. S., and O. P. De Witt, "Thermophysical Properties of Matter," 8, Ed. IFI Plenum (1972).
Wen, C. Y., and Y. H. Yu, "A Generalized Method for Predicting the Minimum Fluidization Velocity," *AIChE J.*, **12**, p. 610 (1966).

Manuscript received October 15, 1980; revision received August 5, and accepted August 24, 1981

Influence of Vapor Entrainment on Distillation Tray Efficiency at High Pressures

P. J. HOEK and F. J. ZUIDERWEG

Laboratory for Process Equipment
Delft University of Technology
Delft, The Netherlands

A recent publication of Fractionation Research Inc. (FRI) (Sakata and Yanagi, 1979) provides experimental evidence that tray efficiency initially rises with increasing pressure, reaches a maximum value, and then decreases again at very high pressures. It is shown in this paper that at these high pressures, significant amounts of vapor can be entrained with the downflowing liquid, e.g., abt. 50 mol per 100 mol liquid at 2,760 kPa. A new model is developed to determine the effect of vapor entrainment on tray efficiency. It is shown that the experimentally observed loss of tray efficiency corresponds with the entrainment rates found at high pressures.

SCOPE

At the Third International Symposium on Distillation in London, Sakata and Yanagi (1979) have reported on pressure drop, capacity, entrainment, weeping and tray efficiency of a commercial size 1.2-m diameter sieve tray. The experiments were carried out with two hydrocarbon systems over a wide range of pressures. This set of FRI data will probably prove to be quite useful for checking existing and developing new tray performance models. During the discussion at the symposium, Porter and Jenkins (1979) pointed out the relevance of the spray regime with regard to the FRI entrainment data.

It is the scope of the present study to offer an explanation for a remarkable trend in the FRI efficiency data; i.e., with increasing pressure, overall tray efficiency first increases but decreases again when the pressure rises over 1,140 kPa (Table 1).

Parallel with the efficiency loss at high pressures the capacity of the sieve tray is also strongly reduced. This can be seen from Figure 1 in which in the usual manner the "capacity factor" is plotted against the "flow parameter."

The loss of tray efficiency at high pressures is surprising, since with increasing pressure most of the physical properties of boiling homogeneous systems become continuously more favorable for enhancing mass transfer. In particular, the interfacial area will become very large because of the rapidly decreasing surface tension which reaches zero value at the critical pressure. Thus, the local point efficiency can be speculated to go up to 100% when the critical point is approached. It is, therefore, important first to analyze the suggested anomaly in the FRI high-pressure efficiency data before these data are used for the development of new tray efficiency correlations.

Sakata and Yanagi mention that at the very high pressures the capacity of the trays is limited by downcomer flooding; i.e., at the onset of flooding, the bed levels are still very low and practically no liquid is entrained with the vapor. This suggests that the downcomers are filled with foam; it is, therefore, conceivable that vapor is entrained with the liquid downflow to the next lower tray. In a recent paper, Lockett and Gharani (1979) confirm that at high downcomer velocities considerable amounts of vapor are entrained. However, they do not expect this entrainment to have a noticeable influence on tray efficiency at high pressures.

In the present study estimates are made on the average vapor content in the downcomer two-phase mixture by calculating the liquid backup at flooding. The resulting vapor entrainment is found by using Lockett and Gharani's (1979) ratio between the downcomer average vapor content and the vapor content of the downcomer underflow. In order to see if the quantities of entrained vapor thus found correspond with the observed efficiency losses, a new vapor entrainment/efficiency model is developed.

CONCLUSIONS AND SIGNIFICANCE

From the calculation of the vapor content in the downcomer two-phase mixture at flooding, it is concluded that at the highest FRI experimental pressures considerable amounts of vapor are entrained with the liquid downflow, e.g., at 2,760 kPa, about 50 kmol vapor per 100 kmol liquid. Further, the calculated entrainment rates correspond with the observed loss in overall tray efficiency under the condition that in the numerical evaluation